Tectonophysics 502 (2011) 315–327

Contents lists available at ScienceDirect

Tectonophysics

journal homepage: www.elsevier.com/locate/tecto

Temperature estimates of coseismic heating in clay-rich fault gouges, the Chelungpu fault zones, Taiwan

Li-Wei Kuo [a], Sheng-Rong Song [a,*], Lin Huang [a], En-Chao Yeh [b], Huei-Fen Chen [c]

[a] Department of Geosciences, National Taiwan University, Taiwan
[b] Department of Earth Sciences, National Taiwan Normal University, Taiwan
[c] Institute of Applied Geosciences, National Taiwan Ocean University, Taiwan

ARTICLE INFO

Article history:
Received 7 August 2010
Received in revised form 20 November 2010
Accepted 1 February 2011

Keywords:
Clay mineral
Temperature estimates
Chelungpu fault
TCDP

ABSTRACT

To investigate the coseismic frictional temperature in seismogenic fault zones, we examine the characteristics of clays in the Chelungpu-fault zones with isothermal heating experiments, scanning electron microscope coupled to an energy dispersive spectrometer (SEM/EDX), and thermogravimetry analysis (TGA). In the TCDP case (Taiwan Chelungpu fault Drilling Project), three fault zones of the Chelungpu-fault system were identified at the depth of 1111 m, 1153 m, and 1222 m (described as FZ1111, FZ1153, and FZ1222 hereafter), respectively. The clay mineral assemblages of FZ1111 show evidence of melting, and the temperature in a ~2 cm band within the black gouge zone is estimated to be from 900 °C to 1100 °C by comparing the SEM images of in situ natural samples with those of heated materials, and the finding of no recrystallization of kaolinite-amorphous aluminosilicates-spinel in the fault samples. The clay mineral assemblages of FZ1153 suggested that kaolinite has been broken down by the thermal decomposition/dehydroxylation but chlorite has not. The clay characteristics and results of SEM/EDX and TGA constrain the faulting temperature from 500 °C to 900 °C, with a spatial distribution up to ~1.3 m. The clay characteristics of FZ1222 indicated that clays were changed by experiencing high temperature acid fluids, instead of thermal decomposition/dehydroxylation processes, and that the temperature is localized in ~2 cm and ranges from 350 °C to 500 °C, the lowest temperature among three fault zones. The estimates of temperature ranges, and thermal anomaly intervals among three fault zones provide important information and constraints on the physical and chemical processes, coseismic dynamic weakening mechanism, and earthquake energy budget in the future.

1. Introduction

The Chelungpu thrust fault is an active fault which slipped on 21st September 1999 with Mw7.6 near Chi-Chi in central Taiwan (Fig. 1). The Chi-Chi earthquake produced a northward propagating rupture with a ~90 km long north–south trending rupture surface (Chen et al., 2001; Lee et al., 2001; Ma et al., 2000). The coseismic slip and rupture velocity increased northward along the fault trace with a slip of 5–9 m horizontal displacement on the northern segment, compared to the average slip of 2 m on the southern part (Chen et al., 2001; Lee et al., 2001; Ma et al., 2000; Yue et al., 2005). In addition, strong ground motion of high-frequency acceleration decreased from south to north (Lin et al., 2001). This N–S trending thrust dips eastward at about 30°, and displacement was nearly pure thrust slip near the epicenter and changed to oblique northward thrust with a strong left-lateral component during the Chi-Chi event (Chen et al., 2001; Dalguer et al., 2001).

After the Chi-Chi earthquake, two shallow drillings across the Chelungpu-fault were carried out at Fengyuan (northern site; the depth of borehole is 455 m) and Nanto (southern site; the depth of borehole is 211 m) to investigate the difference in seismic slip mechanisms between northern and southern fault segments (Tanaka et al., 2002). The clay characteristics of core samples from the Fengyuan borehole suggested that the smectite–illite reaction was a thermal effect by faulting (Liao, 2003). Moreover, old pseudotachylyte of low degree of melting in the core samples was found in the southern site (Otsuki et al., 2005a,b). Hence, Otsuki et al. (2005a) concluded that the faulting mechanism on the northern fault segment was the elastohydrodynamic lubrication, while faulting was restricted by the patches of highly viscous pseudotachylyte melts on the southern segment. Furthermore, the elastohydrodynamic lubrication was postulated that it could work effectively on the northern fault segment shallower than several kilometers (Ma et al., 2003).

In order to obtain more advanced and comprehensive physical and chemical details of the Chelungpu-fault zone, the Taiwan Chelungpu-fault Drilling Project (TCDP) was conducted in 2005. Two holes, named Hole-A and Hole-B with side-track coring, were drilled 6 km south of the Fengyuan site and 2 km east of the surface rupture of the

* Corresponding author at: No. 1, Sec. 4, Roosevelt Road, Taipei, 10617, Taiwan. Fax: +886 2 23636095.
E-mail address: srsong@ntu.edu.tw (S.-R. Song).

0040-1951/$ – see front matter © 2011 Elsevier B.V. All rights reserved.
doi:10.1016/j.tecto.2011.02.001

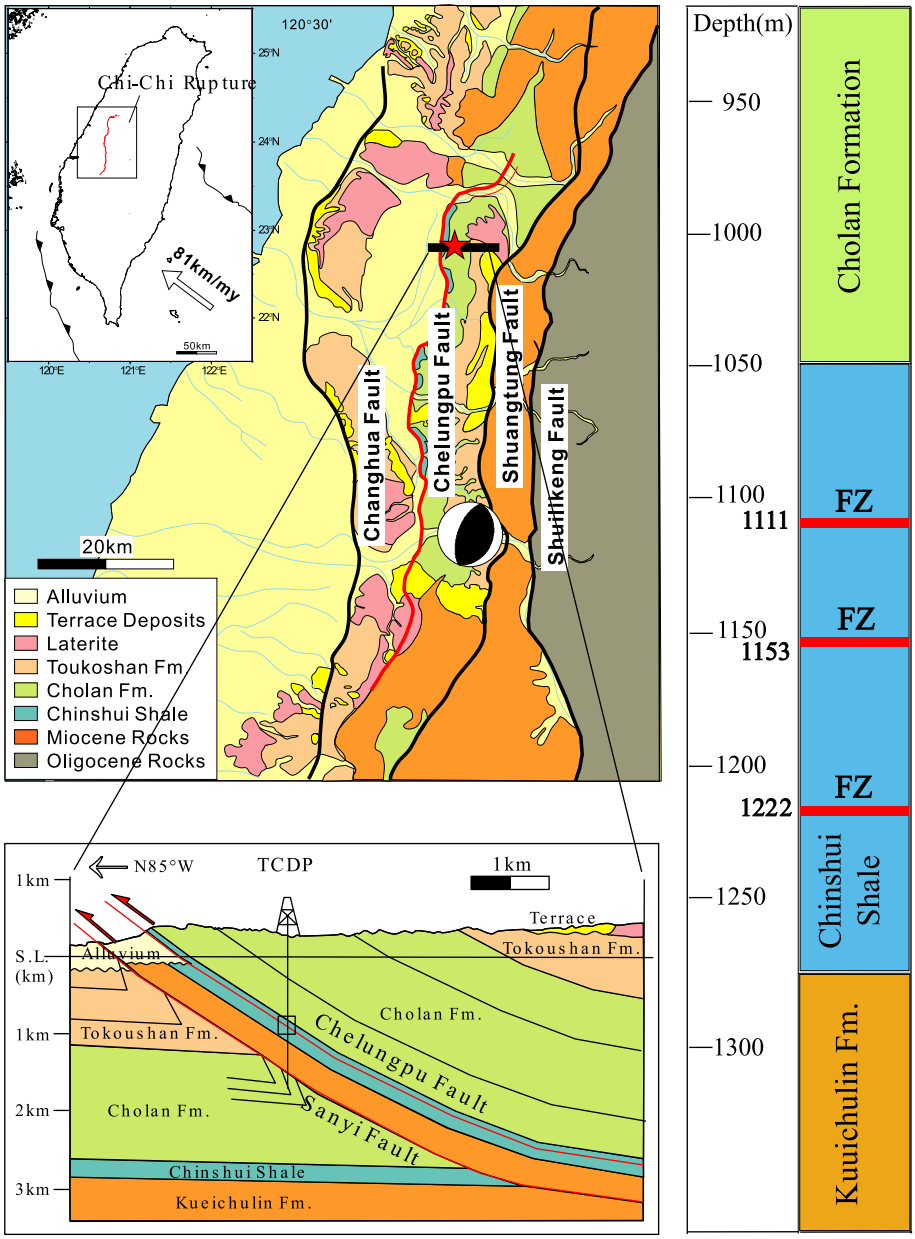

Fig. 1. Geological map of the central part of western Taiwan showing the distribution of formations and major faults. The TCDP site is indicated by a red star. The focal mechanism of the Chi-Chi main shock is located at the hypocenter of the Chi-Chi earthquake. The inset box is the tectonic setting of Taiwan. An E–W cross section displays the relation between formations and faults (after Hung et al., 2007). The rectangle is the Chelungpu-fault and enlarged in the right panel. The image exhibiting major portions of the Chelungpu-fault along the borehole of TCDP. (For interpretation of the references to color in this figure legend, the reader is referred to the web version of this article.)

Chelungpu-fault. Core samples were extracted from 431 m to 2003 m depth for Hole-A, and from 948 m to 1353 m for Hole-B. A general description and fault structures of core samples for Hole-A have been reported by Sone et al. (2007), Song et al. (2007), and Yeh et al. (2007), and those for Hole-B were described by Hirono et al. (2008a). The distance between the two holes is 40 m, and three major fault zones were identified at 1111 m, 1153 m, and 1222 m depth for Hole-A, which correspond to 1136 m, 1194 m, and 1243 m depth for Hole-B. So far, there have been many studies focusing on the shallowest fault zone of the Chelungpu-fault, for example, residual temperature anomaly (Kano et al., 2006), grain size distribution (Ma et al., 2006), geophysical logs (Wu et al., 2007), microstructures (Boullier et al., 2009), and characteristics of clay minerals (Kuo et al., 2009) for Hole-A, and magnetic susceptibility (Hirono et al., 2006a), inorganic carbon content (Hirono et al., 2006b), clay mineral reaction (Hirono et al., 2008b), and microstructures (Boullier et al., 2009) for Hole-B. These different kinds of characteristics indicate that the shallowest fault zone was the Principal Slip Zone (PSZ, established by Sibson (2003)) associated with the 1999 Chi-Chi earthquake, and the faulting mechanism on the shallowest fault zone of the Chelungpu-fault from TCDP was postulated as thermal pressurization based on the observation of microstructures (Boullier et al., 2009), and the observation of clay-clast aggregates (Boutareaud et al., 2010). Moreover, numerical modeling provided by Tanikawa and Shimamoto (2009) along with friction experiments showed that the reduction of stress and instability of fault by thermal pressurization could explain the different behaviors in the northern and southern part of the Chelungpu-fault during the 1999 Chi-Chi earthquake.

Temperature plays an essential role in manipulating earthquake faulting. With frictional heating, the fault strength could be dramatically reduced because of various proposed slip weakening mechanisms, such as frictional melting (Di Toro et al., 2006; Mackenzie and

Brune, 1972), and thermal pressurization (Boullier et al., 2009; Wibberley and Shimamoto, 2005). Also, frictional energy comprises a fair amount of total released earthquake energy (Chester et al., 2005; Scholz, 2002; Sibson, 1973). Therefore, the information regarding a temperature rise by frictional heating in earthquake faults is important for investigating the fault strength and earthquake energy budgets (Di Toro et al., 2005, 2006; Hirose and Shimamoto, 2005). The temperatures of PSZ of the Chelungpu-fault zones for Hole-A and Hole-B during coseismic events were estimated by using magnetic susceptibility (Mishima et al., 2006, 2009), inorganic carbon content (Hirono et al., 2006a), compositions of major and trace elements (Ishikawa et al., 2008), and the occurrence of pseudotachylyte (Otsuki et al., 2009). However, these were either a lower limit (350 °C by Ishikawa et al., 2008; 450 °C by Mishima et al., 2006, 2009; 550 °C by Hirono et al., 2006a), or a wide range (750 °C–1700 °C by Otsuki et al., 2009) for the coseismic events. Those results are too rough to provide more insights into the true faulting mechanisms.

In this study we performed isothermal heating experiments and examined some specific characteristics of clay minerals to place a better constraint on the temperature range of the Chelungpu-fault zones. We also utilize the TGA results of chlorite and kaolinite, and discuss the reactions such as thermal decomposition/dehydroxylation and spinel recrystallization to define the possible temperature range of faulting. This study is intended to provide a better understanding of the faulting temperatures of these three fault zones of the Chelungpu-fault, and also offers important information to investigate the faulting mechanism and to calculate the energy budget.

2. Sampling description

A brittle fault zone can be divided into three major components: fault core, damage zone, and host rock (Chester et al., 1993). The fault core, which accommodates the most slip and reflects high shear strain, is typically characterized by geochemically altered and comminuted rocks such as fault gouge. PSZ mentioned above cut the fault core and is a part of fault core. The damage zone encloses the fault core, and is characterized by an increased density of subsidiary faults, fractures, veins, foliation, and folding relative to the host rock. The host rock, or protolith, surrounding the fault core and damage zone remains basically undamaged during faulting; however, it contains regional structures and also places an important control of background deformation structures and compositions (Caine et al., 1996). In the TCDP case, the thickness of fault cores ranges from millimeters, such as black gouge, to meters, such as gray gouge (Song et al., 2007; Yeh et al., 2007). The black gouge samples of FZ1153 and FZ1222 are ~1 millimeter thick, so it is difficult to collect continuous samples as did Kuo et al. (2009) for FZ1111. Thus, we analyzed only one sample from each black gouge of FZ1153 and FZ1222.

Because shale- and clay-rich fault zones are weathered easily, they are typically not well preserved. On the contrary, the Taiwan Chelungpu-fault Drilling Project collects fresh materials that escaped surficial weathering for examinations of the characteristics of the PSZ of shale-rich fault (Kuo et al., 2009). Therefore, a sequential and continuous collection of fresh samples from host rock to fault core could hopefully provide original characteristics of clay minerals of the Chelungpu-fault zones, and help to determine what the possible thermodynamic processes might have affected these fault zones during coseismic events.

3. Analytical methods

3.1. X-ray diffractometer (XRD)

In our study, a PANalytical X'Pert PRO X-ray diffractometer was used under the conditions of filtered CuKα (1.540 Å) radiation, 45 kV and 40 mA of X-ray generator, 1.0° min^{-1} scanning speed, and 5°–40° of 2θ coverage. We followed the same conditions to prepare the clay samples as described in Kuo et al. (2009) for the other two faults. For identifying and quantifying clay minerals of the clay-size fraction, glass slides of oriented samples were made. All samples were disaggregated in distilled water by using an ultrasonic bath. After centrifugation, draft suspensions of <2 μm were deposited on glass slides. Further, ethylene glycol was used to hydrate the clay samples to recognize swelling clays (smectite and illite/smectite mineral). Clay minerals of <2 μm were determined, and the relative clay mineral percentage was estimated with the semi-quantitative XRD method (Biscaye, 1965). Additionally, to calibrate the proportion of clay minerals in our study, we utilized the mixtures of clay mineral standards (illite (IMt-1), chlorite (ripidolite), and kaolinite (KGa-1)) received from American Clay Mineral Society (Fig. 2).

3.2. Isothermal heating experiment

To estimate the peak temperature and melting texture during the Chi-Chi earthquake, we conducted the isothermal heating experiments (static heating steps in an oven) on the host rock and shale of the Chelungpu-fault. The shale we used is at the depth of 1015.9 m close to the PSZ of the Chelungpu-fault, and the rock in this interval displays no evidence for fracture, comminution, or fluid–rock interaction under naked-eye observation. The mineral assemblages and chemical compositions of shale are assumed to be similar to the original material of black gouge in the fault zone. The shale materials were analyzed with XRD and observed with SEM after isothermal heating experiments. To investigate the influence of temperature on clay mineral change, our target temperatures were set at 600 °C, 700 °C, 800 °C, 900 °C, 1000 °C, and 1100 °C, respectively. The temperature of the oven was set to increase continuously with a heating rate of 150 °C/min to achieve the target temperatures. After reaching the target temperature, it lasted for 10 min, and then cooled down at a rate of 5 °C/min.

3.3. Thermogravimetry analysis (TGA)

Thermogravimetry analysis (TGA) of the clay samples was undertaken by using a METTLER TOLEDO (TGA/SDTA851) thermogravimetry analyzer. The initial TGA temperature for all the samples was 25 °C and the final temperature was 1000 °C. The heating rate was 200 °C/min (the highest rate for this instrument) and the tests were carried out under air purging at a rate of 50 mL/min. In this work, 18–26 mg of material from each clay was thinly spread on a platinum pan and then analyzed by TGA.

3.4. Scanning electron microscope with energy dispersive spectrometer (SEM/EDX)

To identify the major chemical composition of chlorite, we used SEM/EDX quantitative analysis with FEI QUANTA 200 F scanning electron microscope coupled to an energy dispersive spectrometer at 10 kV (SEM/EDX) with the standardized processes from National Taiwan University (NTU).

4. Results

4.1. Characteristics of the clay-rich fault gouge at FZ1111

Previous XRD studies of PSZ clay minerals have suggested that the frictional temperature achieved in the Chi-Chi earthquake was at least 800 °C (Kuo et al., 2009). However, the X-ray energy used in Kuo et al. (2009) was not strong enough to reveal distinctive peaks of informative mineral(s), such as spinel, to better constrain the faulting temperature. In this study we analyzed the PSZ samples with a stronger X-ray generator, which allows low abundance minerals to be revealed, such as spinel, to obtain more information about recrystallization. Then, we combined the new results with those of Kuo et al. (2009) to extend our understanding of faulting temperature by comparing the clay characteristics between fault samples and sedimentary formation. The variability of major

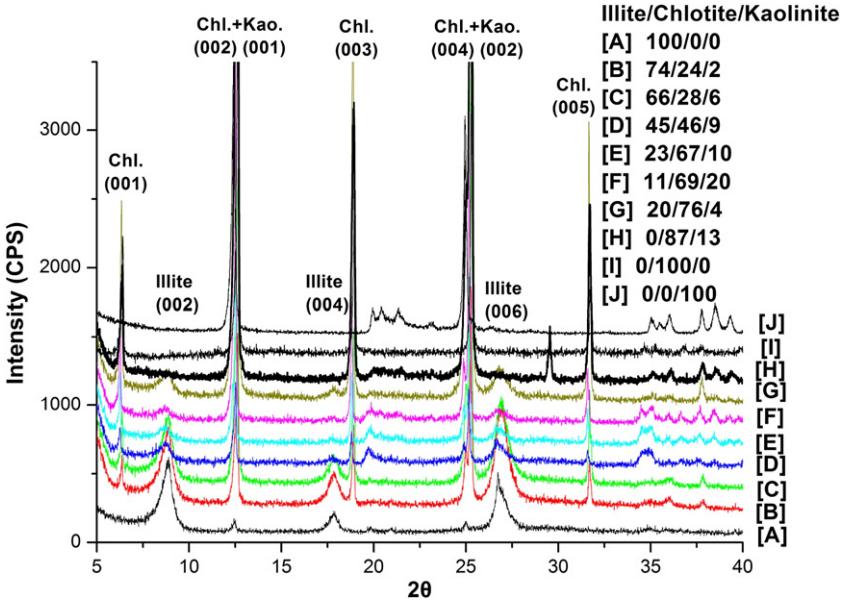

Fig. 2. XRD analysis results of different proportion of clay mineral standards received from American Clay Society.

minerals and clay minerals analyzed with host rocks from 600 m to 1300 m depth are shown in Fig. 3. It seems that the variability of major minerals and clay minerals in Cholan Formation is larger than the ones of Chinshui Shale and upper part of Kueichulin Formation.

The major mineral assemblages via XRD analysis were identified as quartz, feldspar, phyllosilicate minerals, such as illite, smectite, chlorite, and kaolinite (Fig. 4). The variation of illite and chlorite in 1110 m to 1110.5 m depth represents the normal variability of mineral proportion without anomalies of clay minerals proportion. However, the relative percentage and presence of clay minerals vary drastically in 1111.28 m depth. Smectite is present, and its relative percentage increases to 80%; chlorite and kaolinite are absent, and the relative percentage of illite decreases to 20%. After carefully examining the XRD patterns, we do not observe small peaks from low abundance minerals, and conclude that the clay results are the same as described by Kuo et al. (2009).

4.2. Characteristics of the clay-rich fault gouge at FZ1153

To understand the mineral assemblages and the average clay contents of FZ1153, fourteen powdered samples extracted from each part of fault components were examined by XRD analysis (Fig. 5). The relative clay percentage of host rocks was found in a constant range of 20–40%, but drastically decreases to <20% in the fault core (Fig. 5). Clay minerals of <2 μm from our samples are recognized as illite, chlorite, and kaolinite. The relative percentage of illite varies between 50% and 80% for all samples, and there is no smectite in FZA1153 (Fig. 5). The relative percentage of chlorite and kaolinite for all intervals is around 10–20% and 20–40%, respectively, but the content of kaolinite drops to zero in a wide span of ~1.3 m, which includes the entire fault core, regardless of the constituents (black gouge or sandy gouge), and some parts of damaged zone (Fig. 5). The small peak of kaolinite from 1152.2 m to 1152.3 m depth represents the normal variability of mineral proportion instead of the anomaly by faulting.

The XRD patterns of ethylene-glycol samples indicate that no illite/smectite minerals exist throughout the FZ1153 (Fig. 5). This result is different from the findings of surface outcrops (Issacs et al., 2007; Liao, 2003) contaminated by surface weathering processes, but is similar to the results of Kuo et al. (2009). The evidence of low or zero smectite and illite/smectite content in all our samples suggests that no weathering at the depths from which our samples extracted, and useful information about the frictional heat via the characteristics of in situ clay mineralogy could be obtained.

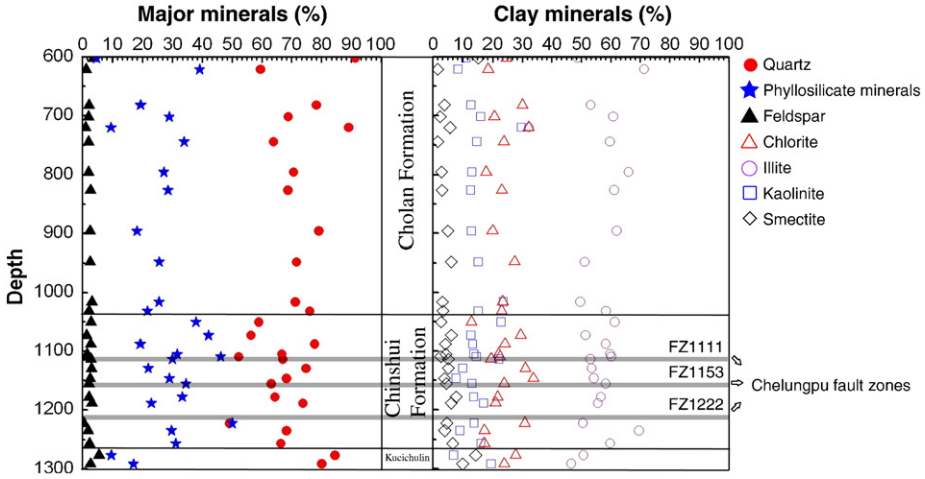

Fig. 3. Results of relative percentage of major minerals and clay minerals from TCDP cores from 600 to 1300 m in depth (after Kuo et al., 2009). Left panel is the plot of major minerals from bulk XRD analysis. Right panel is the result of clay mineral percentages by clay mineral XRD analysis. The three Chelungpu-fault zones are noted as gray areas.

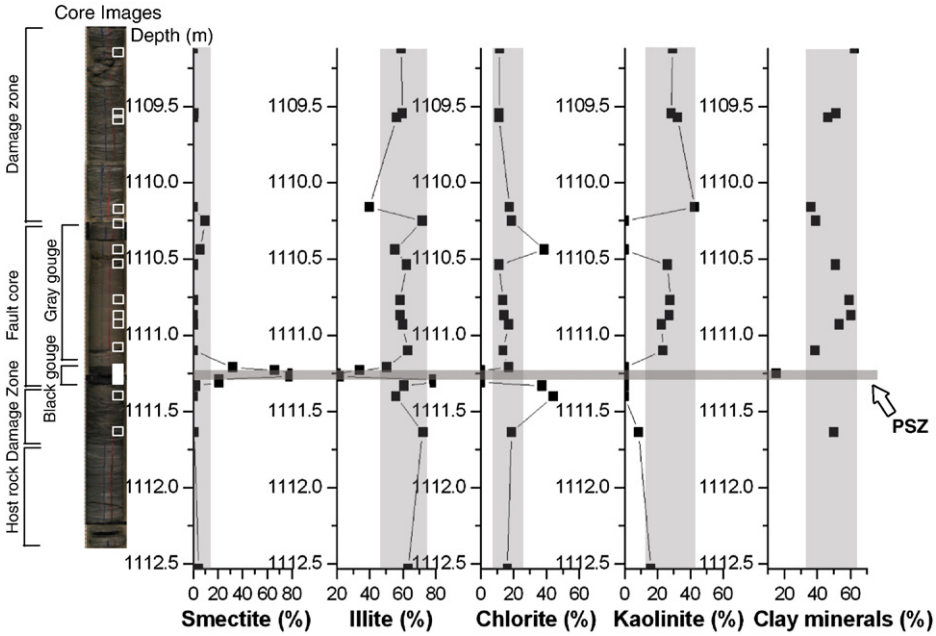

Fig. 4. Clay mineral percentage and interpreted fault components in FZ1111. White rectangles are the sample locations. The results of relative clay mineral percentage by clay mineral XRD analysis are shown in the right side, where illite, smectite, chlorite, and kaolinite are shown by the side. Gray area is the PSZ of the Chi-Chi earthquake.

4.3. Characteristics of the clay-rich fault gouge at FZ1222

The mineral assemblages of FZ1222 were examined by XRD analysis (Fig. 6), and the relative clay percentage of sedimentary formations is found in the constant range of 10–40%. Such a variation in relative clay percentage in FZ1222 is larger than that in FZ1222 and FZ1153, and could have been caused by sandstone-shale interbedding (Fig. 6). Given this lithological variation in FZ1222, it is required to collect samples along the drilled core to minimize the effect of lithological change when identifying the clay anomaly.

Clay minerals (<2 μm) from our FZ1222 samples are recognized as illite, smectite, chlorite, and kaolinite. The relative percentage of illite varies from 60% to 80% for all samples, but abruptly increases to ~90% in the upper black gouge of FZ1222. The relative percentage of chlorite and kaolinite for all intervals is ~8–20% and 9–25%, respectively, but drops to less than 5% in the upper black gouge of FZ1222. Smectite is very uncommon or absent in the Chinshui Shale, but slightly increases in the fault core of FZ1222.

In comparison with the relative clay content of the Chinshui shale, the characteristics of clay minerals in three fault zones are briefly summarized as follows: the 2 cm-thick FZ1111 PSZ has a high content in smectite (90%), kaolinite is absent within 1.3 m around FZ1153 and the relative percentage of clays slightly varies in the FZ1222 black gouge.

4.4. Isothermal heating experiment

Here we cannot perform the experiments at a heating rate (e.g., 200 °C/s) as fast as faulting does due to the instrumental limitation, nor can we conduct experiments to evaluate the effect of pressure, loading and fluid. Given that the heating rate and pressure/loading

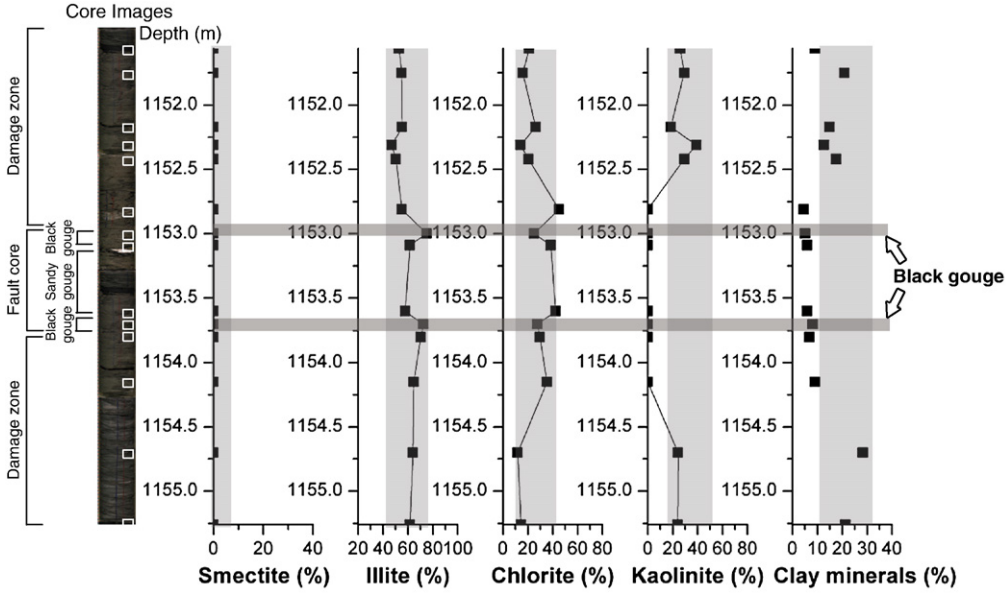

Fig. 5. Clay mineral percentage and interpreted fault components in FZ1153. White rectangles are the sample locations. The results of relative clay mineral percentage by clay mineral XRD analysis are shown in the right side, where illite, smectite, chlorite, and kaolinite are shown by the side. Gray areas are shown as the possible slip zones of Chelungpu fault.

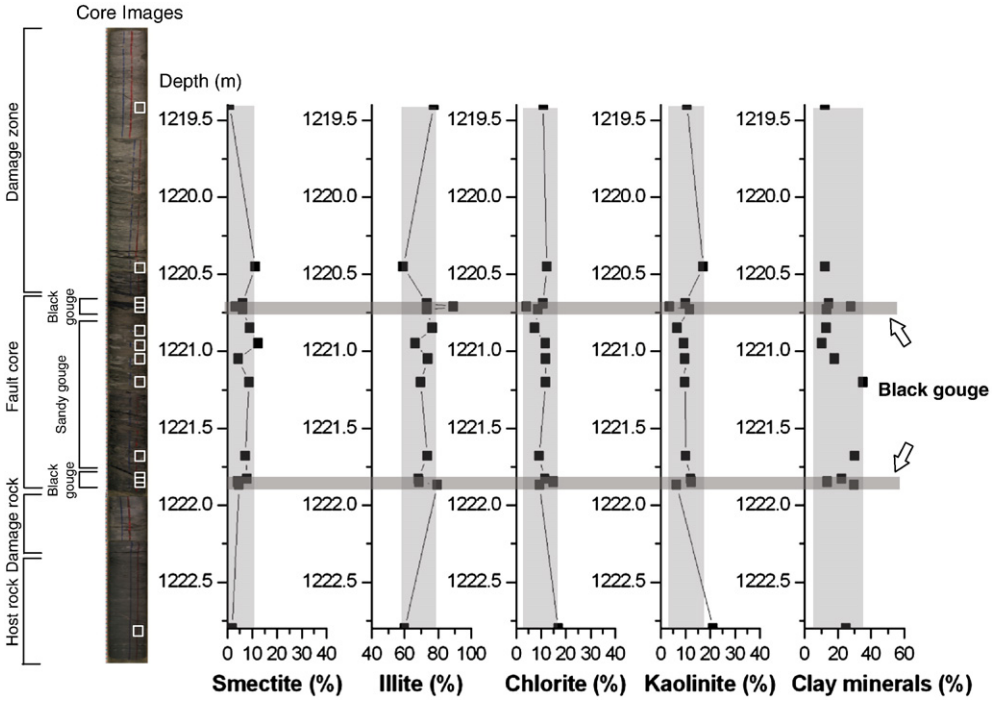

Fig. 6. Clay mineral percentage and interpreted fault components in FZ1221. White rectangles are the sample locations. The results of relative clay mineral percentage by clay mineral XRD analysis are shown in the right side, where illite, smectite, chlorite, and kaolinite are shown by the side. Gray areas are shown as the possible slip zone of Chelungpu fault.

can make great influences on the thermal history of fault zones, how thermal decomposition/dehydroxylation of clay minerals could be affected by these parameters will be discussed later. However, results of our isothermal heating experiments can still be used to illustrate and compare the difference in characteristics of clays in the fault zone when different temperatures are achieved during coseismic events.

Our XRD results of the isothermal heating experiments are shown in Fig. 7. The original major mineral assemblages of Chinshui shale via bulk XRD analyses are quartz, feldspar, and phyllosilicate minerals such as muscovite/illite, smectite, kaolinite and chlorite, and no apparent peaks of spinel were found in the XRD patterns of PSZ (Fig. 7A,B). After the isothermal heating experiments, several features were found in the XRD patterns (Fig. 7C–H). The peaks of kaolinite are not present after 600 °C (Fig. 7C), which might have been due to thermal decomposition/dehydroxylation of kaolinite that occurs at T = 500 °C to 550 °C (Killingley and Day, 1990; Temuujin et al., 1998). We cannot observe the peaks of chlorite after 900 °C in XRD patterns (Fig. 7E) because of thermal decomposition of chlorite at T = 600 °C to 900 °C, depending on the chemical composition (Brindley and Ali, 1950; Caillère and Hénin, 1960; Nutting, 1943). Illite is more resistant to high temperature than other clay minerals until T > 900 °C (Fig. 7F). Fig. 6G shows that quartz and feldspar still exist after T > 1000 °C. When the temperature achieves 1100 °C, spinel appears, due to recrystallization of decomposed kaolinite.

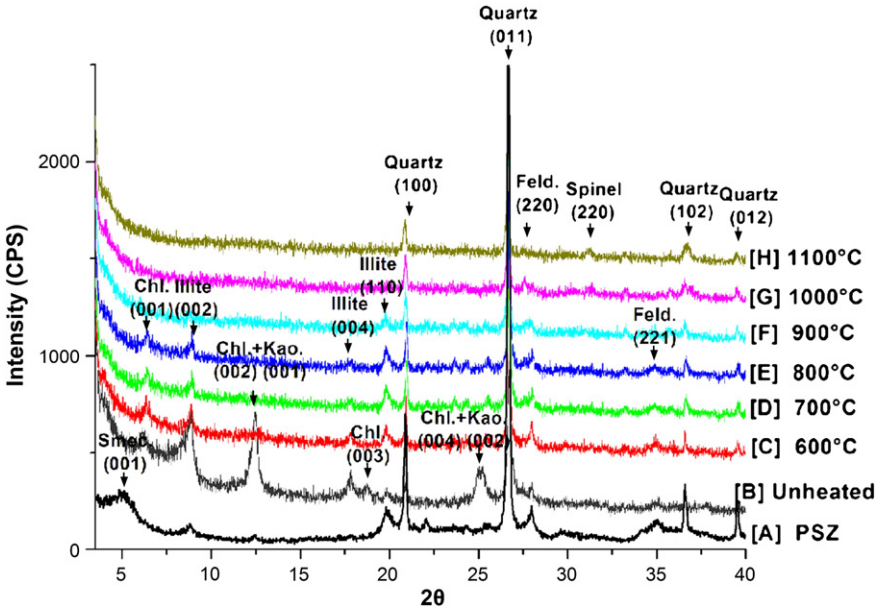

Fig. 7. Comparison of XRD analyses between the PSZ sample and isothermal heating materials. The all apparent peaks are identified with CuKα radiation (the wavelength is 1.5406 Å) and signed with mineral names. (Chl.: chlorite, Kao.: Kaolinite, Smec.: Smectite, and Feld.: feldspar).

Besides, the XRD patterns of heated samples in Fig. 7 show that Mg-chlorite are abundant, and the evidence of the presence of Mg-chlorite includes: (a) odd *hkl* reflections are not stronger than even *hkl* reflections; (b) the presence of even *hkl* reflections; (c) heating to 700 °C does not intensify the (001) reflection and diminish the other peaks; and (d) the change of chlorite heated-treated at 800 °C to a red-brownish breakdown product interpreted as an iron-oxide colored silicate.

We could estimate the possible temperature of faulting through SEM observations of microstructures of heated materials, and comparing them with the natural PSZ samples. Fig. 8A shows the original surface texture collected from the PSZ of the Chelungpu-fault. Many vesicles about 1 to 20 μm across were identified, indicating that this sample must have melted as described by Kuo et al. (2009). Fig. 8B shows the original surface texture obtained from Chinshui shale. The disorder flakes of clay minerals were observed, and no obvious melting occurrence was noted. The SEM images of heated materials at T = 600 °C, 700 °C, and 800 °C (Fig. 8C–E) show similar surface textures to the one of Fig. 8B; whereas the heated samples at T = 900 °C, 1000 °C, and 1100 °C (Fig. 8F–H) show many vesicles which are ~1- to 3-μm, 1- to 10-μm, and 1- to 50-μm across, respectively. This demonstrates that vesicles become larger with higher temperatures in the normal pressure.

4.5. Thermogravimetry analysis (TGA)

Thermogravimetry determines the temperature at which thermal reactions take place in an object when it is heated continuously to an elevated temperature, and the intensity and general characteristics of such reactions.

To clearly observe the curves of thermal decomposition/dehydroxylation of clays, we used clay samples, instead of whole rocks, for identification with XRD. Of four clay samples used in this TGA study, three were American Clay Mineral Society Source Clay, which are illite (IMt-1) (Fig. 9a), chlorite (ripidolite) (Fig. 9b), and kaolinite (KGa-1) (Fig. 9c), and the fourth one was extracted from the host rock shale (the mixtures composed of illite, chlorite, kaolinite, and little smectite) (Fig. 9d). Pure smectite samples were not analyzed with TGA because of its low abundance in our study.

The TGA results of clays illustrate characteristics of thermal decomposition/dehydroxylation with high heating rates. In the case of the clay minerals, simultaneous differential thermal analyses (SDTA) show characteristic endothermic reactions due to dehydration or thermal decomposition/dehydroxylation and to loss of crystal structure, and exothermic reactions usually due to the formation of new phases at elevated temperatures (Brindley and Nakahira, 1959). The dehydration and thermal decomposition/dehydroxylation curve for illite is given in Fig. 9a. The curve remains flat up to ~220 °C, then drops gradually until T ~ 440 °C due to water loss. Significant water loss occurs at T = 440 °C ~ 940 °C (−4.16%). The SDTA result (−16.6 °C) of illite is given in Fig. 9a, which shows a wide range of endothermic reactions from the room temperature to the target temperature. The curve of thermal decomposition/dehydroxylation for chlorite is shown in Fig. 9b. The curve has an almost flat top up to about ~580 °C, and two steps of considerable weight losses at T = 580 °C to 745 °C (−6.25%), and T = 745 °C to 920 °C (−3.00%), respectively. The SDTA result (−8.9 °C and −6.5 °C) of chlorite is given in Fig. 9b, and it displays several wide ranges of endothermic reactions overlapped with the high heating rate. The curve of thermal decomposition/dehydroxylation for kaolinite is shown in Fig. 9c. It shows a single step of weight loss, which is observed from 480 °C to 920 °C (−13.70%). The SDTA result (−9.4 °C and −11.9 °C) of kaolinite is given in Fig. 9c, and it displays several wide ranges of endothermic reactions overlapped with the high heating rate. The dehydration and thermal decomposition/dehydroxylation curve for the mixtures of clays from Chinshui is given in Fig. 9d. It shows a similar curve to the ones of illite that are almost flat up to about ~120 °C, then drop gradually due to water loss up to about 350 °C (−2.61%), and considerable loss between 350 °C to 940 °C (−10.58%). The SDTA result of the mixtures of clays from Chinshui is given in Fig. 9d, which shows one considerable endothermic reaction from the room temperature to about 600 °C and one slight endothermic reaction from 600 °C to the target temperature.

4.6. Scanning electron microscope with energy dispersive spectrometer (SEM/EDX)

The thermal decomposition/dehydroxylation temperature of chlorite is dependent on crystallinity, grain size, and the most important, chemical compositions (the Fe/Mg ratio) (Caillère and Hénin, 1960; Nutting, 1943). We extracted clay samples from the Chinshui shale, and performed EDX quantitative line scans of the selected area without carbon coating, to examine the distribution of the elements in chlorite.

Aggregates of clay minerals are present in our clay sample extracted from shale (Fig. 10). Three quantitative line scans of the selected area were taken to investigate the chemical composition of clay. SEM/EDS detected O^{2-}, Al^{3+}, Si^{4+}, Fe^{3+}, Mg^{2+}, K^{+}, and C^{4+} in the aggregates of clay minerals (Table 1). C^{4+} is the major component of carbon tapes for sticking clay powders. Area 1 (spectrum 1) shows the peaks of O, Si, Al, K, Mg, and Fe, which may correspond to illite and some chlorite. Area 2 (spectrum 2) and area 3 (spectrum 3) only show the peaks of O, Si, Al, and Mg, indicating that the aggregates are mainly composed of Mg-chlorite (Fig. 10).

5. Discussion

5.1. Estimate of the maximum temperature achieved in FZ1111

The SEM images described in the previous section suggest that clay minerals within ~2 cm of PSZ were melted (Fig. 7A). It was also concluded by Kuo et al. (2009) that the temperature of faulting was roughly inferred to be over 800 °C due to the thermal dehydroxylation of chlorite by frictional heating (Brindley and Ali, 1950). However, the temperature of thermal dehydroxylation of chlorite varies with different crystallinity, grain size, and chemical compositions (Fe–Mg) (Caillère and Hénin, 1960; Nutting, 1943). Therefore, in this study we carried out the isothermal heating experiments and XRD analysis of heated material (Fig. 7), observed the surface melting with SEM (Fig. 8), and identified the major type of chlorite semi-quantitatively with SEM/EDX (Fig. 10) to investigate the maximum temperature achieved in the fault zones. The change of mineral assemblages by different heating temperatures can be clearly observed in Fig. 7. The PSZ mineral assemblages of FZ1111 include quartz, feldspar, rare illite, abundant smectite (Fig. 7A), and the presence of clay minerals is similar to that of the heated materials at T = 900 °C (Fig. 7F) despite the fact that much of smectite formed from alteration of glasses (Kuo et al., 2009). The similar mineral assemblage between PSZ and the materials heated at 900 °C may suggest that 900 °C might be achieved by faulting in coseismic events in the PSZ of FZ1111. Therefore, it suggests that the lower bound (900 °C) of FZ1111 is higher than what Kuo et al. (2009) suggested. Besides, it should be noted that the presence of spinel is observed in the heated materials at 1100 °C (Fig. 7H), and the presence of spinel is the result of recrystallization of kaolinite achieved at 1100 °C (Traoré et al., 2006). After thermal decomposition/dehydroxylation of kaolinite, the decomposed kaolinite remains as a secondary mineral, such as amorphous aluminosilicates, and these amorphous aluminosilicates could recrystallize into spinel when temperature increases to 1100 °C (Traoré et al., 2006). The lack of spinel peak in the XRD pattern of the PSZ of FZ1111 (Fig. 7A) indicates that such recrystallization of kaolinite did not happen in the PSZ of FZ1111, and therefore suggests that the

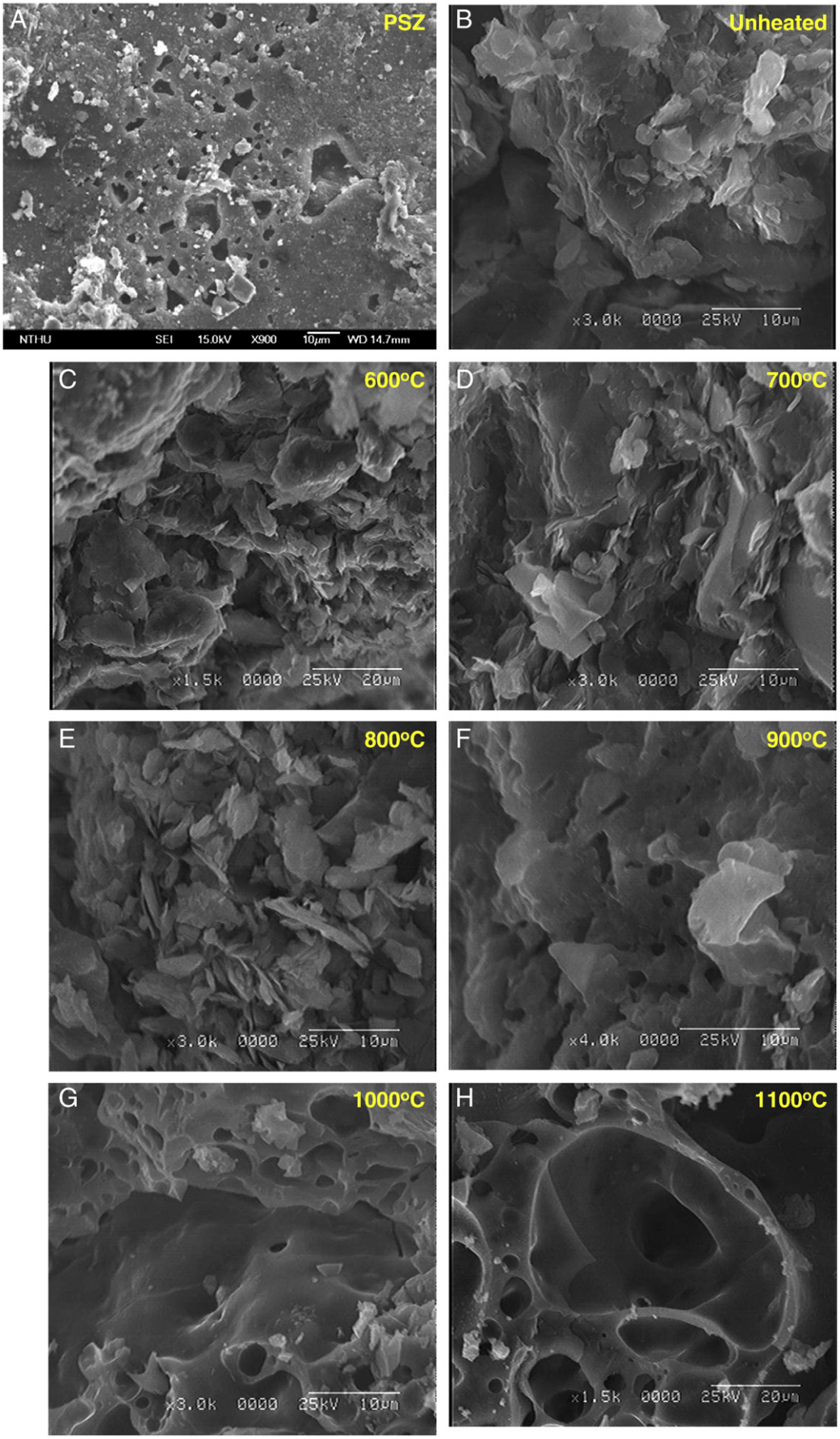

Fig. 8. SEM images of the PSZ and isothermal heating materials. It is noted that vesicles appear at 900 °C, and the vesicles become larger within increasing temperatures.

temperature did not achieve 1100 °C during faulting. Thus, 1100 °C could be considered the upper bound of temperature by seismic slip.

The various surface textures of heated material at different experimental temperatures can be used as a reference to which in situ materials of fault zones can be compared. The appearance of vesicles on the surface of heated samples is important for identifying melting occurrence via increasing temperatures. The original host rocks contain flake-shaped minerals, such as phyllosilicates, and granular-shaped minerals, such as quartz (Fig. 8B). The vesicles on the surface were not formed in heated materials until 900 °C (Fig. 8F). These vesicles on the surface grew larger after 900 °C (Fig. 8G–H). By comparing the size of vesicles on the surface of the PSZ of FZ1111 with the experimental results, we infer that the temperature in the PSZ of FZ1111 might have been above 900 °C. This is indeed consistent with what is inferred from the correlation of isothermal heating materials XRD patterns, and suggests that 900 °C is the lower temperature limit of FZ1111. It should be noted that the pressure was not probed in this work, and should be considered to be another important factor to affect the size of vesicles in the future studies.

It is interesting to compare our results with previous studies. The results of clay mineral of Hole-B were interpreted in terms of dehydroxylation of kaolinite and dehydration of interlayer water, dehydroxylation, and illitization of smectite occurred during coseismic frictional heating (Hirono et al., 2008b). It implies that the temperature of faulting was not high enough to cause melting that we mentioned here. The different characteristics of clay minerals in the fault zone between Hole-A and Hole-B can be interpreted as a result of heterogeneous frictional heating on the fault surface caused by different asperities (Childs et al., 2008), even though they are only 40 m away.

On the other hand, it seems that the illitization of smectite did not occur in Hole-A of TCDP. The reaction of smectite to illite in sedimentary basins is well documented and considered a classic reaction of clastic diagenesis (Abercrombie et al., 1994). The reaction seems to rely on five variables: 1) time, 2) heat, 3) the availability of K^+, 4) fluids, and 5) confining pressures and water pressures (Moore and Reynolds, 1997; Velde et al., 1986; Whitney, 1990). Several studies have presented that seismic energy (shear stress and coseismic heat flow) overcomes the kinetic barrier and drives smectite to illite reactions (Evans and Chester, 1995; Vrolijk and van der Pluijm, 1999; Wintsch et al., 1995). Thermodynamic modeling of smectite to illite with consideration of temperature, pressure, and water activity, was also considered (Dubacq et al., 2010; Vidal and Dubacq, 2009). However, given the very short time of heating by faulting and lab friction experiments with high velocity and high heating rates that failed to trigger clay reactions (Boutareaud et al., 2010), the reaction of smectite–illite mentioned above seems to be caused mostly by low heating rate processes (diagenesis). It strongly suggests that normal thermal decomposition/dehydroxylation, instead of high heating rate caused by faulting, might have been the driving force for the reaction of smectite to illite. This mechanism might explain why the illitization of smectite is not observed (Hole-A) or not complete (Hole-B) after careful examinations of the characteristics of clay minerals from TCDP (Hirono et al., 2008b; Kuo et al., 2009).

5.2. Estimate of the maximum temperature achieved in FZ1153

The clay results of XRD show that the disappearance of kaolinite was located in a relatively wider interval ~1.3 m of FZ1153 (compared to the clay anomaly of FZ1111) (Fig. 5), and the relative percentage of clay minerals is lower than the average one of Chinshui formation at the same interval. The occurrence of kaolinite might have been caused by thermal decomposition/dehydroxylation because of frictional heating during earthquakes, and this absence of kaolinite is also observed in the materials that experienced high velocity rotary shear experiments (Brantut et al., 2008). We could observe that the significant thermal decomposition/dehydroxylation of kaolinite with a high heating rate (200 °C/min) from TGA analysis begins at 580 °C (Fig. 9c). The results of TGA in this study are different from the ones done with a normal heating rate (20 °C/min) (Killingley and Day, 1990; Temuujin et al., 1998). This observation is consistent with the hypothesis that the temperature of thermal decomposition/dehydroxylation is controlled by heating rates (Sembira and Dunn, 1996). On the other hand, the variation in heating rates on the endothermic reaction for kaolinite indicates that in general, the slower the heating rate, the broader the peak and the lower the temperature of the peak (e.g., 5 °C/min to 20 °C/min) (Spiel et al., 1945). However, the result of SDTA in our study (Fig. 9c) show two broad peaks instead of one single sharp peak seen in Spiel et al. (1945). Combining the results of TGA and SDTA, it strongly suggests that the reaction of thermal decomposition/dehydroxylation is varied at high heating rates. Therefore, the thermal decomposition/dehydroxylation of kaolinite with a normal heating rate is proposed at T = 500 °C to 550 °C (Killingley and Day, 1990; Temuujin et al., 1998), and we are estimating a truthful temperature range of faulting during coseismic events. Thus, we set 500 °C as a lower bound of temperature on FZ1153 when faulting.

Additionally, we discuss more details about chlorite with our results of SEM/EDX, TGA, and several previous studies to estimate the temperature range of thermal dehydroxylation of chlorite in the fault zone. Nutting (1943) reported several dehydroxylation curves for different chlorites, and some of them showed a gradual continuous loss of weight from about 600 °C to 850 °C, where dehydroxylation is essentially complete. Meanwhile, other chlorites studied in Nutting (1943) show a relatively slight loss between 600 °C and about 750 °C to 800 °C, and then a relatively abrupt loss from 800 °C to essentially complete dehydroxylation at 850 °C to 900 °C. The experiments show that the dehydroxylation characteristics of chlorite vary with composition. The data of dehydroxylation temperature for chlorite with various cations in the octahedral layers were also provided by Caillère and Hénin (1960). Their data indicate that the dehydroxylation temperature of Mg-chlorite (820 °C) is higher than that of Fe-chlorite (530 °C). Therefore, identification of chemical composition of chlorite is critical to estimating the thermal records during faulting. The results of SEM/EDX show that the mixtures of clay extracted from Chinshui shale are composed of illite (spectrum 1) and Mg-chlorite (spectra 2 and 3) (Fig. 10). The TGA curve of chlorite shows (Fig. 9b) that the reaction of thermal decomposition/dehydroxylation takes place from 580 °C to 920 °C. The TGA curve of chlorite is also different from the results of previous studies presumably because of high heating rate (Caillère and Hénin, 1960; Nutting, 1943).

Moreover, analysis of individual and collective reflections of chlorite XRD pattern as shown by Grim (1968) and Carroll (1970) indicates that the chlorite in our study is a trioctahedral Mg-rich chlorite, and contains essentially no iron. These observations and results show that Mg-rich chlorite, instead of Fe-rich chlorite, is dominant in our samples, and imply that the estimated complete dehydroxylation temperature of chlorite should be 900 °C. Hashimoto et al. (2008) have documented that Mg-chlorite is abundant in the samples of Hole-B, and interpreted the negligible amount of Fe-chlorite in the black gouge as the clay anomaly due to fluid–rock interaction and thermal decomposition. Comparing with the clay results of Hole-A and Hole-B, the presence of Mg-chlorite indicates different thermal effects during coseismic events in TCDP case.

Thermal decomposition/dehydroxylation of kaolinite and chlorite mentioned above were all conducted at 1 atm. Yeskis et al. (1985) showed that the dehydroxylation of kaolinite varies with different pressures in high pressure DTA experiments (20 °C/min). The dehydroxylation temperature of kaolinite is 525 °C (1 bar), 627 °C (30.5 bar), and 670 °C (5270 bar) under an inert pressurizing medium with argon, whereas the temperature is 650 °C (46.5 bar), 520 °C (1088 bar), and 571 °C (5716 bar) under an inert pressurizing medium with water. Bai

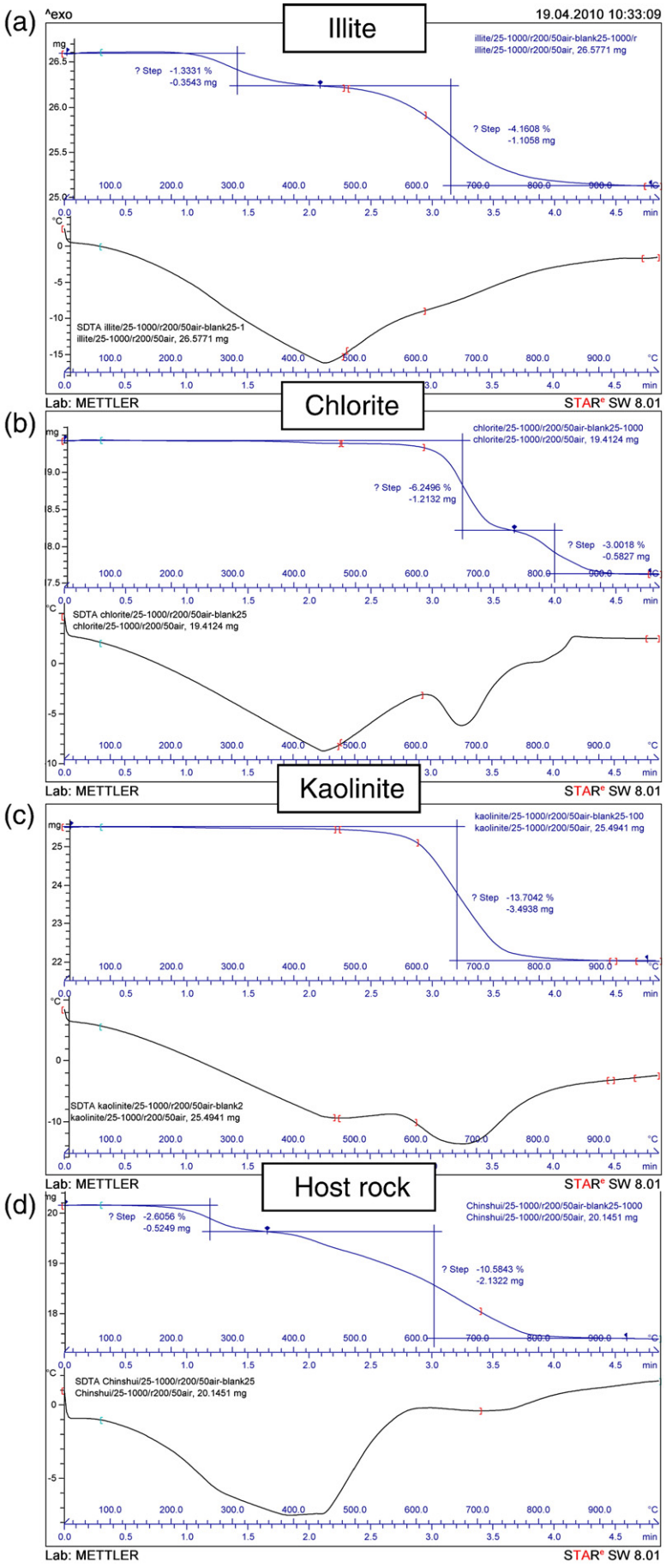
(a)
Illite
^exo
19.04.2010 10:33:09
illite/25-1000/r200/50air-blank25-1000/r
illite/25-1000/r200/50air, 26.5771 mg
? Step -1.3331 %
-0.3543 mg
? Step -4.1608 %
-1.1058 mg
SDTA illite/25-1000/r200/50air-blank25-1
illite/25-1000/r200/50air, 26.5771 mg
Lab: METTLER
STARe SW 8.01
(b)
Chlorite
chlorite/25-1000/r200/50air-blank25-1000
chlorite/25-1000/r200/50air, 19.4124 mg
? Step -6.2496 %
-1.2132 mg
? Step -3.0018 %
-0.5827 mg
SDTA chlorite/25-1000/r200/50air-blank25
chlorite/25-1000/r200/50air, 19.4124 mg
Lab: METTLER
STARe SW 8.01
(c)
Kaolinite
kaolinite/25-1000/r200/50air-blank25-100
kaolinite/25-1000/r200/50air, 25.4941 mg
? Step -13.7042 %
-3.4938 mg
SDTA kaolinite/25-1000/r200/50air-blank2
kaolinite/25-1000/r200/50air, 25.4941 mg
Lab: METTLER
STARe SW 8.01
(d)
Host rock
Chinshui/25-1000/r200/50air-blank25-1000
Chinshui/25-1000/r200/50air, 20.1451 mg
? Step -2.6056 %
-0.5249 mg
? Step -10.5843 %
-2.1322 mg
SDTA Chinshui/25-1000/r200/50air-blank25
Chinshui/25-1000/r200/50air, 20.1451 mg
Lab: METTLER
STARe SW 8.01

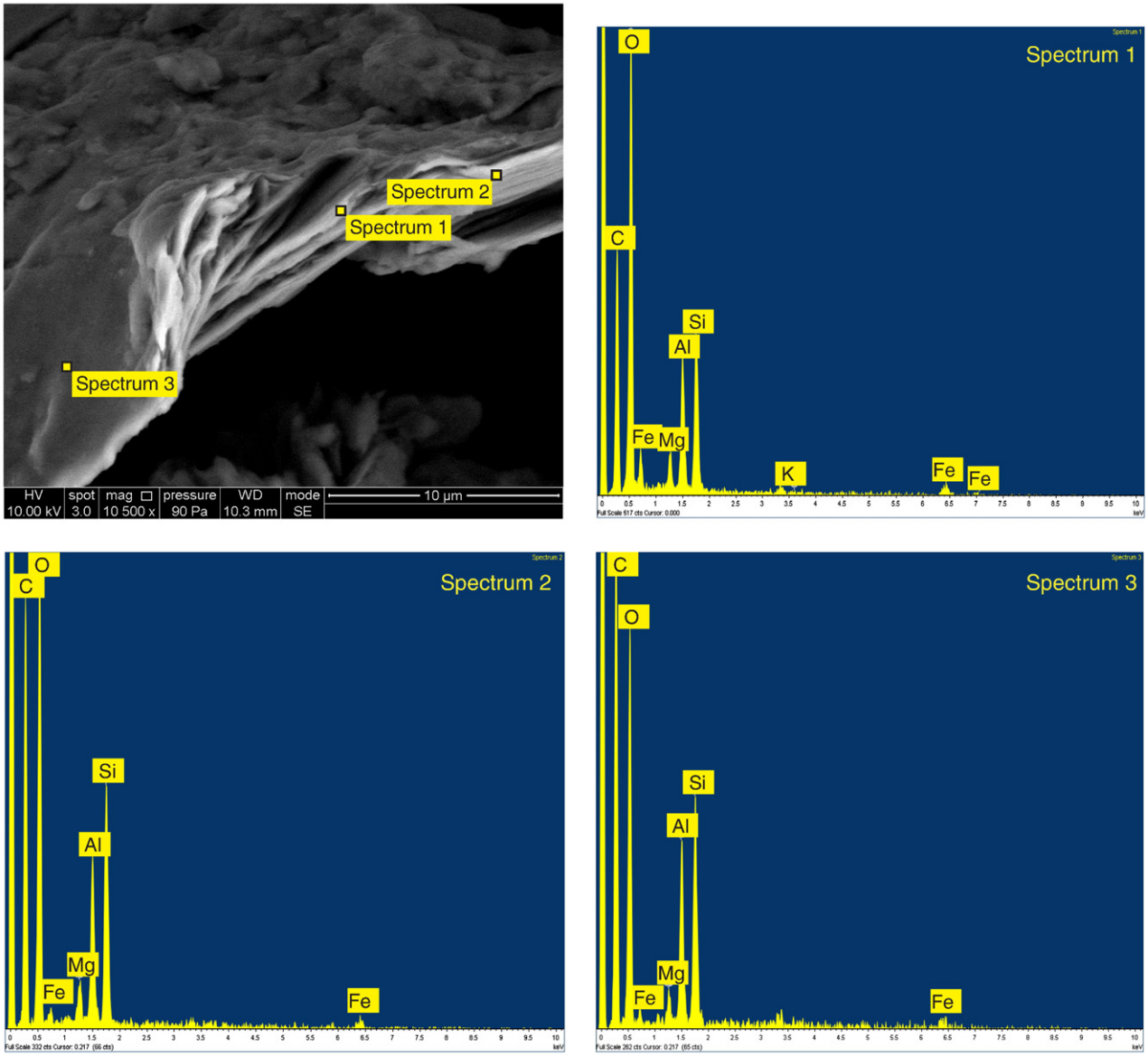

Fig. 10. SEM image and EDS analyses of a section of the aggregates of clay minerals extracted from Chinshui shale. Note that the oxides of Mg appear adjacent to the center part of the aggregates of clay minerals. The oxides of K and Fe are negligible amount in spectra 2 and 3.

et al. (1993) reported that the dehydroxylation temperature of chlorite varied from 738 °C to 869 °C (1 bar to 770 bar) in closed capsules. These studies indicate that the pressure and water partial pressure are important factors of thermal decomposition/dehydroxylation, and that the difference in thermal decomposition/dehydroxylation between kaolinite and chlorite is small at high pressures as discussed above. In the TCDP case, the pores are located at 1 km depth, which translates to an equivalent surrounding pressure of 100 bar. Based on the interpolation of high pressure DTA experiments in previous studies (Bai et al., 1993; Yeskis et al., 1985), the temperature of thermal decomposition/dehydroxylation is 620 °C (kaolinite), 770 °C (Fe-chlorite), and 855 °C (Mg-chlorite), respectively. The temperature range between kaolinite and chlorite under 100 bar is smaller than what we offer under the normal pressure. Therefore, our inferred temperature range could be considered a conservative estimate, and thus should be applicable to high pressure conditions (5.7 kbar for kaolinite and 0.7 kbar for chlorite).

Furthermore, the XRD results of isothermal heating experiments are showing that total thermal dehydroxylation of chlorite occurs at T = 900 °C (Fig. 7). It indicates that the temperature of thermal dehydroxylation of chlorite in the Chinshui shale is lower than 900 °C. Hence, from the characteristics of clay minerals, thermal decomposition/dehydroxylation between kaolinite and chlorite, and the comparison between XRD results of FZ1153 and of isothermal heating experiments, it is a conclusive result that the temperature of FZ1153 achieved 500 °C to 900 °C during coseismic events.

5.3. Estimate of the maximum temperature achieved in FZ1222

In contrast to FZ1111 and FZ1153, FZ1222 seems to have no obvious clay anomalies of lower clay mineral percentage and clay dehydroxylation driven by large frictional heat (Fig. 6). However, a notable phenomenon in FZ1222 is that the relative percentage of illite increases

Fig. 9. TGA (right upper rectangle) and SDTA (right lower rectangle) results of three standard clay minerals and one clay samples from Chinshui shale. They are (a) illite, (b) chlorite, (c) kaolinite, and (d) the host rock (illite, chlorite, and kaolinite) from Chinshui shale. (The XRD results of three standard clay minerals and one clay samples from Chinshui shale before heating are shown as Fig. 2A, I, J and 7B, respectively).

Table 1
Element contents determined by SEM/EDX analysis on the clay samples from shale.

Spectrum	C	O	Mg	Al	Si	K	Fe	Total
Spectrum 1	29.03	36.00	1.79	6.60	8.90	1.43	16.26	100.00
Spectrum 2	46.44	35.34	1.38	6.25	10.59			100.00
Spectrum 3	50.95	31.74	1.05	6.92	9.34			100.00

to almost 90%, but that of smectite, chlorite, and kaolinite slightly decreases in the upper black gouge zone of ~2 cm interval. We propose that frictional heating and acid fluids may play a role in initiating the smectite to illite reaction and chlorite vanishing reaction in the black gouge zone to increase relative percentage of illite, but decrease that of smectite and chlorite (Huang et al., 1993; Moore and Reynolds, 1997; Senkayi et al., 1981; Vrolijk and van der Pluijm, 1999). Here we focus on the discussion of heat source and its temperature range for this hypothesis. First, the temperature record of TCDP-A was 46.5 °C at 1200 m depth along the bore hole (Kano et al., 2006). It is much lower than the temperature (100 °C–150 °C) of smectite to illite transformation (Freed and Peacor, 1989; Hyndman, 2004). Second, if considering the smectite to illite reaction at T = 100 °C to 150 °C (the maximum burial temperature, Freed and Peacor, 1989; Hyndman, 2004; Yue et al., 2005), the clay mineral assemblages in our samples should show a similar trend within the diagenesis process. The clay mineral anomaly in FZ1222 was localized in ~2 cm interval instead of being widely distributed. It suggests that diagenesis is not the main process to drive the smectite to illite reaction. Last, relative clay percentages in FZ1222 are not lower than the ones of Chinshui, which means that no thermal decomposition/dehydroxylation occurred. Therefore, frictional energy produced by coseismic events is the most possible heat source to drive smectite to transfer to illite, instead of thermal decomposition/dehydroxylation during diagenesis. Furthermore, the temperature constraint provided from TCDP Hole-B suggests that high temperature fluid (>350 °C) has interacted with fault core material (Ishikawa et al., 2008). However, chlorite is in a stable phase and should not be depleted in this temperature range. Therefore, the consumption of chlorite in our study may be related to acid fluid (Senkayi et al., 1981). We propose that chlorite in fault gouge might have been altered by acid fluid and have further transferred to trioctahedral smectite or dissolved (Senkayi et al., 1981). Thus, the reaction of smectite–illite and the consumption of chlorite with assisting high temperature acid fluid caused by frictional heat were probably proceeded to produce the occurrence of rich illite and less smectite and chlorite in FZ1222. The hot acid fluids interacted in FZ1222 may be due to the thermal heat pulse during coseismic slip.

5.4. Limitation of temperature estimate and its significance

In this study, we utilize the breakdown temperature of clay minerals to estimate the peak temperature in coseismic events. However, the fault surfaces were not only heated, but they are also rubbed and grinded during frictional sliding in the same time. Rubbing induces tribochemical reactions which include mechanically and thermally activated reactions. Tribochemical reactions result in the formation of new compounds and trigger dehydroxylation and dehydration reactions in the case of clays, and they also induce different reaction mechanisms. It suggests that tribochemical reactions may occur at lower activation energies (and thus their kinetics is more efficient at a given temperature) than thermo-chemical reactions (Steinike and Tkácová, 2000). Thus, considering the effects of tribochemical reaction, the determined temperature range for three fault zones, or the highest temperature achieved in the slipping zone, might be overestimated. Here we present the approaching temperature estimates instead of lower bounds provided in the past, and these estimates may provide constraints on the studies of (i) the physical and chemical processes activated during seismic slip, (ii) the activation of coseismic dynamic weakening mechanism and, more in general, and (iii) earthquake energy budget for the Chelungpu fault.

6. Conclusion

The temperatures among three fault zones of the Chelungpu-fault estimated from the characteristics of clay minerals and implications are provided, and they are summarized as follow: (1) temperature range of FZ1111 was from 900 °C to 1100 °C and clay anomalies were localized in a narrow zone (2 cm), (2) temperature range of FZ1153 was from 500 °C to 900 °C and the clay anomalies were widely distributed in a wide interval (~1.3 m), and (3) temperature range in FZ1222 was between 350 °C and 500 °C and clay change via high temperature fluid–rock interaction occurred in the upper black gouge zone (~2 cm). Thus, we suggest that these clay characteristics of the fault zones could provide important thermal constraints for investigation of the Chelungpu fault during coseismic events.

Acknowledgements

We thank two anonymous reviewers for their many positive and constructive comments, and we also thank Chief Editor Hans Thybo for editing this paper and giving valuable comments. We thank the working group of TCDP, including the drilling company FangYu and WanDa, the on-site assistants and participating students from NTU and NCU. We also thank M.C. Liu for English polishing. We thank H. C. Shiao for offering XRD standard data. This research was supported by the National Science Council of Taiwan under grant NSC 96-2627-M-002-011 and NSC 98-2627-M-002-002.

References

Abercrombie, H.J., Hutcheon, I.E., Bloch, J.D., de Caritat, P., 1994. Silica activity and the smectite–illite reaction. Geology 22 (6), 539–542.
Bai, T.B., Guggenheim, S., Wang, S.J., 1993. Metastable phase relations in the chlorite–H_2O system. American Mineralogist 78, 1208–1216.
Biscaye, P.E., 1965. Mineralogy and sedimentation of recent deep-sea clays in the Atlantic Ocean and adjacent seas and oceans. Geological Society of America Bulletin 76, 803–832.
Boullier, A.M., Yeh, E.C., Boutareaud, S., Song, S.R., Tsai, C.H., 2009. Micro-scale anatomy of the 1999 Chi-Chi earthquake fault zone. Geochemistry Geophysics Geosystems 10 (3), Q03016.
Boutareaud, S., Boullier, A.M., Andréani, M., Calugaru, D.G., Beck, P., Song, S.R., Shimamoto, T., 2010. Clay clast aggregates in gouges: new textural evidence for seismic faulting. Journal of Geophysical Research 115, B02408. doi:10.1029/2008jb006254.
Brantut, N., Schubnel, A., Rouzaud, J.N., Brunet, F., Shimamoto, T., 2008. High-velocity frictional properties of a clay-bearing fault gouge and implications for earthquake mechanics. Journal of Geophysical Research 113, B10401. doi:10.1029/2007JB005551.
Brindley, G.W., Ali, S.Z., 1950. Thermal transformations in magnesium chlorites. Acta Crystallographica 3, 25–30.
Brindley, G.W., Nakahira, M., 1959. The kaolinite–mullite reaction series. Journal of the American Ceramic Society 42, 311–324.
Caillère, S., Hénin, S., 1960. Relationship between the crystallochemical constitution of phyllites and their dehydration temperature, application in the case of chlorites. Bulletin of Society France Ceramic 48, 63–67.
Caine, J.S., Evans, J.P., Forster, C.B., 1996. Fault zone architecture and permeability structure. Geology 24 (11), 1025–1028.
Carroll, D., 1970. Clay Minerals: A Guide to Their X-raxy Identification.
Chen, Y.G., Chen, W.S., Lee, J.C., Lee, Y.H., Lee, C.T., Chang, H.C., Lo, H.C., 2001. Surface rupture of 1999 Chi-Chi earthquake yields insights on active tectonics of central Taiwan. Bulletin of Seismological Society of America 91, 977–985.
Chester, F.M., Evans, J.P., Biegel, R.L., 1993. Internal structure and weakening mechanisms of the San Andreas Fault. Journal of Geophysical Research 98, 771–786.
Chester, J.S., Chester, F.M., Kronenberg, A.K., 2005. Fracture surface energy of the Punchbowl fault, San Andreas system. Nature 437, 133–136.
Childs, C., Manzocchi, T., Walsh, J.J., Bonson, C.G., Nicol, A., Schöpfer, M.P.J., 2008. A geometric model of fault zone and fault rock thickness variations. Journal of Structural Geology 31 (2), 117–127.
Dalguer, L.A., Irikura, J.D., Riera, J.D., Chiu, H.C., 2001. The importance of the dynamic source effects on strong ground motion during the 1999 Chi-Chi, Taiwan, earthquake: brief interpretation of the damage distribution on building. Bulletin of Seismological Society of America 91, 1112–1127.

Di Toro, G., Pennacchioni, G., Teza, G., 2005. Can pseudotachylytes be used to infer earthquake source parameters? An example of limitations in the study of exhumed faults. Tectonophysics 402, 3–20.
Di Toro, G., Hirose, T., Nielsen, S., Pennacchioni, G., Shimamoto, T., 2006. Natural and experimental evidence of melt lubrication of faults during earthquakes. Science 31, 647–649.
Dubacq, B., Vidal, O., Andrade, V.D., 2010. Dehydration of dioctahedral aluminous phyllosilicates: thermodynamic modelling and implications for thermobarometric estimates. Contributions to Mineralogy and Petrology 159, 159–174. doi:10.1007/s00410-009-0421-6.
Evans, J.P., Chester, F.M., 1995. Fluid–rock interaction in faults of the San Andreas system: inferences from San Gabriel fault rock geochemistry and microstructures. Journal of Geophysical Research 100, 13,007–13,020.
Freed, R.L., Peacor, D.R., 1989. Variability in temperature of the smectite/illite reaction in Gulf Coast sediments. Clay Minerals 24 (2), 171–180.
Grim, R.E., 1968. Clay Mineralogy, 2nd ed. McGraw-Hill, New York.
Hashimoto, Y., Tadai, O., Tanimizu, M., Tanikawa, W., Hirono, T., Lin, W., Mishima, T., Sakaguchi, M., Soh, W., Song, S.R., Aoike, K., Ishikawa, T., Murayama, M., Fujimoto, K., Fukuchi, T., Ikehara, M., Ito, H., Kikuta, H., Kinoshita, M., Masuda, K., Matsubara, T., Matsubayashi, O., Mizoguchi, M., Nakamura, N., Otsuki, K., Shimamoto, T., Sone, H., Takahashi, M., 2008. Characteristics of chlorites in seismogenic fault zones: the Taiwan Chelungpu Fault Drilling Project (TCDP) core sample, e-Earth 3. http://www.electronic-earth.net/3/issue1.html2008p. 1–6.
Hirono, T., Lin, W., Yeh, E.C., Soh, W., Hashimoto, Y., Sone, H., Matsubayashi, O., Aoike, K., Ito, H., Kinoshita, M., Murayama, M., Song, S.R., Ma, K.F., Hung, J.H., Wang, C.Y., Tsai, Y.B., 2006a. High magnetic susceptibility of fault gouge within Taiwan Chelungpu fault: nondestructive continuous measurements of physical and chemical properties in fault rocks recovered from Hole B, TCDP. Geophysical Research Letters 33, L15303. doi:10.1029/2006GL026133.
Hirono, T., Ikehara, M., Otsuki, K., Mishima, T., Sakaguchi, M., Soh, W., Omori, M., Lin, W., Yeh, E.C., Tanikawa, W., Wang, C.Y., 2006b. Evidence of frictional melting within disk-shaped black materials discovered from the Taiwan Chelungpu fault system. Geophysical Research Letters 33, L19311. doi:10.1029/2006GL027329.
Hirono, T., Sakaguchi, M., Otsuki, K., Sone, H., Fujimoto, K., Mishima, T., Lin, W., Tanikawa, W., Tanimizu, M., Soh, W., Yeh, E.C., Song, S.R., 2008a. Characterization of slip zone associated with the 1999 Taiwan Chi-Chi earthquake: X-ray CT image analyses and microstructural observations of the Taiwan Chelungpu fault. Tectonophysics 449, 63–84.
Hirono, T., Fujimoto, K., Yokoyama, T., Hamada, Y., Tanikawa, W., Tadai, O., Mishima, T., Tanimizu, M., Lin, W., Soh, W., Song, S.R., 2008b. Clay mineral reactions caused by frictional heating during an earthquake: an example from the Taiwan Chelungpu fault. Geophysical Research Letters 35, L16303. doi:10.1029/2008GL034476.
Hirose, T., Shimamoto, T., 2005. Slip-weakening distance of faults during frictional melting as inferred from experimental and natural pseudotachylytes. Bullettin of the Seismological Society of America 95, 1666–1673.
Hung, J.H., Wu, Y.H., Yeh, E.C., Wang, J.C., 2007. Subsurface structure, physical properties, and fault zone characteristics in the scientific drill holes of Taiwan Chelungpu-Fault Drilling Project. Terrestrial Atmospheric and Oceanic Science 18, 271–293.
Huang, W.H., Longo, J.M., Pevear, D.R., 1993. An experimental derived kinetic model for the smectite-to-illite conversion and its use as a geothermometer. Clays and Clay Minerals 41, 162–177.
Hyndman, R.D., 2004. Controls on subduction thrust earthquakes: downdip changes in composition and state. In: Karner, G.D., Taylor, B., Driscoll, N.W., Kohlstedt, D.L. (Eds.), Rheology and Deformation of the Lithosphere at Continental Margins. Columbia University Press, New York, pp. 166–178.
Ishikawa, T., Tanimizu, M., Nagaishi, K., Matsuoka, J., Tadai, O., Sakaguchi, M., Hirono, T., Mishima, T., Tanikawa, W., Lin, W., Kikuta, H., Soh, W., Song, S.R., 2008. Coseismic fluid–rock interactions at high temperatures in the Chelungpu fault. Nature Geoscience 1. doi:10.1038/ngeo308.
Issacs, A.J., Evans, J.P., Song, S.R., Kolesar, P.T., 2007. Characterizing brittle deformation, damage parameters, and clay composition in fault zones: variations along strike and with depth in the Chelungpu Fault zone. Terrestrial Atmospheric and Oceanic Science 18, 183–221.
Kano, Y., Mori, J., Fujio, R., Ito, H., Yanagidani, T., Nakao, S., Ma, K.F., 2006. Heat signature on the Chelungpu fault associated with the 1999 Chi-Chi, Taiwan earthquake. Geophysical Research Letters 33, L14306. doi:10.1029/2006GL026733.
Killingley, J.S., Day, S.J., 1990. Dehydroxylation kinetics of kaolinite and montmorillonite. Fuel 69 (10), 1145–1149.
Kuo, L.W., Song, S.R., Yeh, E.C., Chen, H.F., 2009. Clay mineral anomalies in the fault zone of Chelungpu Fault, Taiwan, and its implication. Geophysical Research Letters 36, L18306. doi:10.1029/2009GL039269.
Lee, J.C., Chen, Y.G., Sieh, K., Mueller, K., Chen, W.S., Chu, H.T., Chan, Y.C., Rubin, C., Yates, R., 2001. A vertical exposure of the 1999 surface rupture of the Chelungpu fault at Wufeng, western Taiwan: structural and paleoseismic implications for an active thrust fault. Bulletin of the Seismological Society of America 91 (5), 914–929.
Liao, C. F., 2003. Analysis of fault rock deformation and clay minerals from fault cores of Chelungpu fault zone, Master's thesis of National Central University, in Chinese, summary in English, p. 132.
Lin, A., Ouchi, T., Chen, A., Maruyama, T., 2001. Co-seismic displacements, folding and shortening structures along the Chelungpu surface repture zone occurred during the 1999 Chi-Chi, Taiwan earthquake. Tectonophyics 330, 225–244.
Ma, K.F., Song, T.R.A., Lee, S.J., Wu, H.I., 2000. Spatial slip distribution of the September 20, 1999, Chi-Chi, Taiwan, earthquake, M_w 7.6 — inverted from teleseismic data. Geophysical Research Letters 27, 3417–3420.
Ma, K.F., Brodsky, E.E., Mori, J., Ji, C., Song, T.A., Kanamori, H., 2003. Evidence for fault lubrication during the 1999 Chi-Chi, Taiwan, earthquake (Mw 7.6). Geophysical Research Letters 30, 1244. doi:10.1029/2002/2002GL015380.
Ma, K.F., Tanaka, H., Song, S.R., Wang, C.Y., Hung, J.H., Tsai, Y.B., Mori, J., Song, Y.F., Yeh, E.C., Soh, W., Sone, H., Kuo, L.W., Wu, H.Y., 2006. Slip zone and energetics of a large earthquake from the Taiwan Chelungpu-fault Drilling Project. Nature 444, 473–476.
Mackenzie, D., Brune, J.N., 1972. Melting on fault planes during large earthquakes. Geophysical Journal Royal Astronomical Society 29, 65–78.
Mishima, T., Hirono, T., Soh, W., Song, S.R., 2006. Thermal history estimation of the Taiwan Chelungpu fault using rock-magnetic methods. Geophysical Research Letters 33, L23311.
Mishima, T., Hirono, T., Nakamura, N., Tanikawa, W., Soh, W., Song, S.R., 2009. Changes to magnetic minerals caused by frictional heating during the 1999 Taiwan Chi-Chi earthquake. Earth, Planets, and Space Letters 61, 797–801.
Moore Jr., D.M., Reynolds, R.C., 1997. Chapter 5: Individual Clay Minerals, X-ray Diffraction and the Identification and Analysis of Clay Minerals. Oxford University Press, New York.
Nutting, P.G., 1943. Some standard thermal dehydration curves of minerals. U. S. Geological Survey, Profess paper 197E, pp. 197–216.
Otsuki, K., Uduki, T., Monzawa, N., Tanaka, H., 2005a. Clay injection veins and pseudotachylyte from two boreholes penetrating the Chelungpu fault, Taiwan: their implications for the contrastive seismic slip behaviors during the 1999 Chi-Chi earthquake. The Island Arc 14, 22–36.
Otsuki, K., Uduki, T., Monzawa, N., Tanaka, H., 2005b. Fractal size and spatial distributions of fault zones: an investigation into the seismic Chelungpu fault, Taiwan. The Island Arc 14, 12–21.
Otsuki, K., Hirono, T., Omori, M., Sagaguchi, M., Tanigawa, W., Lin, W., Soh, W., Song, S.R., 2009. Analyses of pseudotachylyte from Hole-B of Taiwan Chelungpu Fault Drilling Project (TCDP); their implications for seismic slip behaviors during the 1999 Chi-Chi earthquake. Tectonophysics. doi:10.1016/j.tecto.2009.01.008.
Scholz, C.H., 2002. The Mechanics of Earthquakes and Faulting, 2nd ed.
Sembira, A.N., Dunn, J.G., 1996. High temperature calibration of DTA and DSC apparatus using encapsulated samples. Thermochimica 274, 113–124.
Senkayi, A.L., Dixon, J.B., Hossner, L.R., 1981. Transformation of chlorite to smectite through regularly interstratified intermediates. Soil Science Society of America Journal 45, 650–656.
Sibson, R.H., 1973. Interaction between temperature and pore-fluid pressure during earthquake faulting—a mechanism for partial or total stress relief. Nature Physical Sicence 243, 66–68.
Sibson, R.H., 2003. Thickness of the seismic slip zone. Bulletin of the Seismological Society of America 93 (3), 1169–1178.
Sone, H., Yeh, E.C., Nakaya, T., Hung, J.H., Ma, K.F., Wang, C.Y., Song, S.R., Shimamoto, T., 2007. Mesoscopic structural observations of cores from the Chelungpu fault system, Taiwan Chelungpu-fault Drilling Project Hole-A, Taiwan. Terrestrial Atmospheric and Oceanic Science 18, 359–377.
Song, S.R., Kuo, L.W., Yeh, E.C., Wang, C.Y., Hung, J.H., Ma, K.F., 2007. Characteristics of the lithology, fault-related rocks and fault zone structures in the TCDP Hole-A. Terrestrial Atmospheric and Oceanic Science 18, 243–269.
Spiel, S., Berkelheimer, L.H., Pask, J.A., Davies, B., 1945. Differential thermal analysis—its application to clays and other aluminous minerals. Bulletin and Technical Papers of the United States Bureau of Mines, p. 664.
Steinike, U., Tkácová, K., 2000. Mechanochemistry of solids—real structure and reactivity. Journal of Materials Synthesis and Processing 8 (3-4), 197–203.
Tanaka, H., Wang, C.Y., Chen, W.M., Sakaguchi, A., Ujie, K., Ito, H., Ando, M., 2002. Initial science report of shallow drilling penetrating into the Chelungpu fault zone, Taiwan. Terrestrial Atmospheric and Oceanic Science 13, 227–251.
Tanikawa, W., Shimamoto, T., 2009. Frictional and transport properties of the Chelungpu fault from shallow borehole data and their correlation with seismic behavior during the 1999 Chi-Chi earthquake. Journal of Geophysical Research 114, B01402. doi:10.1029/2008JB005750.
Temuujin, J., Okada, K., Mackenzie, K.J.D., Jadambaa, T., 1998. The effect of water vapor atmospheres on the thermal transformation of kaolinite investigated by XRD, FTIR and solid state MAS NMR. Journal of the European Ceramic Society 19, 105–112.
Traoré, K., Gridi-Bennadji, F., Blanchart, P., 2006. Significance of kinetic theories on the recrystallization of kaolinite. Thermochimica Acta 451, 99–104.
Velde, B., Suzuki, T., Nicot, E., 1986. Pressure–temperature–composition of illite/smectite mixed-layer minerals: niger delta mudstones and other examples. Clay and Clay Minerals 34 (4), 435–441.
Vidal, O., Dubacq, B., 2009. Thermodynamic modelling of clay dehydration, stability and compositional evolution with temperature, pressure and H_2O activity. Geochimica et Cosmochimica Acta 73, 6544–6564.
Vrolijk, P., van der Pluijm, B.A., 1999. Clay gouge. Journal of Structural Geology 21, 1039–1048.
Whitney, G., 1990. Role of water in the smectite-to-illite reaction. Clays and Clay Minerals 38 (4), 343–350.
Wibberley, C.A.J., Shimamoto, T., 2005. Earthquake slip weakening and asperities explained by thermal pressurization. Nature 436, 689–692.
Wintsch, R.P., Christofferson, R., Kronenberg, A.K., 1995. Fluid–rock reaction weakening of fault zones. Journary of Geophysical Research 100 (B7), 13021–13032.
Wu, H., Ma, K.F., Zoback, M., Boness, N., Ito, H., Hung, J., Hickman, S., 2007. Stress orientations of Taiwan Chelungpu-fault Drilling Project (TCDP) hole-A as observed from geophysical logs. Geophysical Research Letters 34, L01303. doi:10.1029/2006GL028050.
Yeh, E.C., Sone, H., Nakaya, T., Ian, K.H., Song, S.R., Hung, J.H., Lin, W., Hirono, T., Wang, C.Y., Ma, K.F., Soh, W., Kinoshita, M., 2007. Core description and characteristics of fault zones from the Hole-A of the Taiwan Chelungpu-Fault Drilling Project. Terrestrial Atmospheric and Oceanic Science 18, 327–357.
Yeskis, D., Koster van Groos, A.F., Guggenheim, S., 1985. The dehydroxylation of kaolinite. American Mineralogist 70, 159–164.
Yue, L.F., Suppe, J., Hung, J.H., 2005. Structural geology of a classic thrust belt earthquake: the 1999 Chi-Chi earthquake Taiwan (Mw = 7.6). Journal of Structural Geology 27, 2058–2083.